



Observation and modeling of inner divertor re-attachment in discharges with lithium coatings in NSTX

Filippo Scotti^{a,*}, V.A. Soukhanovskii^b, M.L. Adams^b, H.A. Scott^b, H.W. Kugel^a, R. Kaita^a, A.L. Roquemore^a

^a Princeton Plasma Physics Laboratory, Princeton, NJ 08543, United States

^b Lawrence Livermore National Laboratory, Livermore, CA 94550, United States

ARTICLE INFO

Article history:

Available online 19 December 2010

ABSTRACT

In the National Spherical Torus Experiment (NSTX), modifications to the inner divertor plasma regimes are observed in high triangularity, H-mode, NBI heated discharges due to lithium coatings evaporated on the plasma facing components. In particular, the drop in the recombination rate, the reduced neutral pressure and the reduced electron density (inferred from Stark broadening measurements of high- n deuterium Balmer lines) suggested that the inner divertor, which is usually detached in discharges without lithium, re-attached. Experimental results are compared to simulations obtained with a 1D partially ionized plasma transport model integrated in the non-local thermodynamic equilibrium radiation transport code CRETIN to understand how the reduced recycling affects the divertor parameters in NSTX discharges with lithium coatings.

© 2011 Elsevier B.V. All rights reserved.

1. Introduction

In diverted tokamak configurations, ballooning-type radial transport, geometrical effects and cross field drift play a role in producing an in–out asymmetry in the divertor power and particle fluxes [1]. This power difference and the ease of achieving radiative regimes makes the peak heat flux at the inner divertor less of a constraint for divertor design. In spherical tori (STs) this asymmetry is enhanced by the presence of a recycling surface (the center stack) close to the inboard last closed flux surface (LCFS). This is the case also in the National Spherical Torus Experiment (NSTX) where a strong difference between the inboard and outboard scrape off layer (SOL) and divertor regimes is generally observed [2]. The high heat flux together with the small radius and short connection length from midplane to the divertor plate make the achievement of radiative regimes challenging in the outer divertor while, on the other hand, the inner divertor usually detaches early in the discharge.

Lithium wall conditioning by means of evaporative coatings in NSTX modified both the inner and outer divertor regimes [3]. In particular, in highly shaped, high power plasma discharges the generally detached inner divertor re-attached after lithium was evaporated onto the lower divertor, while the SOL transport regime in the outer divertor, which is usually in a high recycling regime, transitioned to a low recycling regime.

Another observation in lithium conditioned discharges was the disappearance of X-point multifaceted asymmetric radiation from

the edge (MARFE), which is thought to have a degrading effect on NSTX performance. While on one hand the disappearance of MARFEs can lead to longer discharge durations, the re-attachment of the inner leg might bring issues linked to the lifetime of the materials under a higher heat flux when we project current machines to a future steady state magnetic fusion reactor. A deeper understanding of NSTX divertor regimes with reduced recycling is desirable.

In this paper, the modifications in the inner divertor due to lithium deposition are analyzed. The experimental observation of the changes in the divertor parameters are presented. We also report on simulations of NSTX divertor re-attachment using a 1-D partially ionized plasma model PIP [4], integrated in the non-local thermodynamic equilibrium (NLTE) radiation transport code CRETIN [5].

2. Experimental setup, observations and method

NSTX is a mid-size, low aspect ratio tokamak ($R = 0.85$ m, $a = 0.68$ m). In this paper, long pulse (up to 1.3 s), H-mode, NBI heated (4–6 MW) discharges were analyzed. Typical conditions of these discharges included: $I_p = 900$ kA, $B_t = 0.45$ T, $T_e(0) \sim 1$ keV, $n_e(0) = 3\text{--}5 \times 10^{13}$ cm⁻³, high elongation ($\kappa = 2.3$) and high triangularity ($\delta = 0.8$). A lower divertor biased double null configuration was used with $\delta_{rsep} = -7$ mm, the inner strike point (ISP) on the center stack and the outer strike point (OSP) on the horizontal divertor plate. In Fig. 1, time traces of several discharge parameters are shown for a pre-lithium discharge (black line) and a post-lithium discharge (red line) with 190 mg of lithium deposited onto the plasma facing components (PFCs).

* Corresponding author.

E-mail address: fscotti@pppl.gov (F. Scotti).

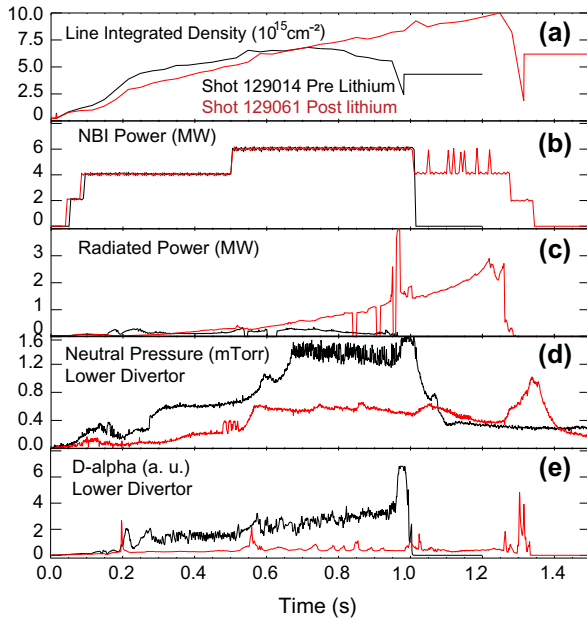


Fig. 1. Time traces of average line density \bar{n}_e (a), auxiliary NBI heating power P_{NBI} (b), core radiated power P_{RAD} (c), neutral pressure in the lower divertor P_{neutr} (d) and $D-\alpha$ emission from the lower divertor I_z (e) for a discharge before lithium deposition (black) and one after lithium deposition on the plasma facing components (red). (For interpretation of the references to color in this figure legend, the reader is referred to the web version of this article.)

Spectroscopic data analyzed in this paper were acquired by means of a 0.5 m UV–VIS spectrometer [6]. The instrumental function in the UV region was about 0.11 nm. In particular, Balmer series spectra (from excited states $n \geq 6$) were analyzed from the chord at $R = 0.31$ m looking through the inner divertor, as shown in Fig. 2 [6]. Neutral pressure in the divertor region was monitored by means of a Penning gauge situated in the lower divertor, below the outer strike point [7]. In the discharges analyzed in this paper, electron densities in the inner divertor were inferred from Stark broadening of high- n deuterium Balmer line radiation $n = 2-6, \dots, 10$ (from now on indicated simply as B6–B10).

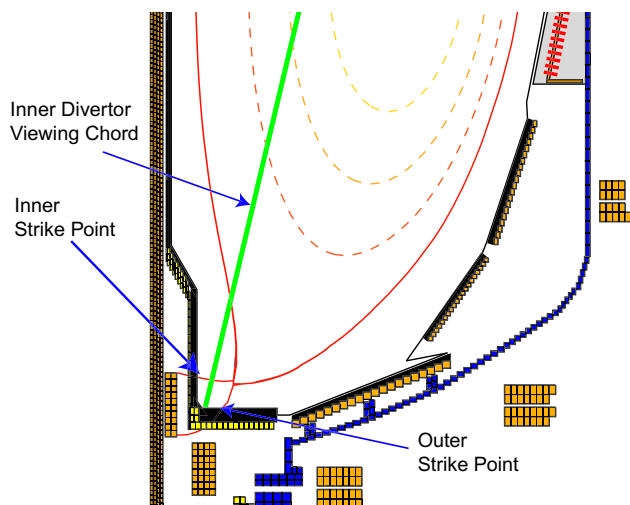


Fig. 2. Schematic of NSTX divertor region. The last closed flux surface is also shown for a high elongation, high triangularity NSTX discharge. The viewing chord used in the spectroscopic data acquisition through the inner divertor is shown in green. (For interpretation of the references to color in this figure legend, the reader is referred to the web version of this article.)

The NLTE radiation transport code CRETIN [5] was used to simulate NSTX deuterium Balmer spectra. The optical depth for an atomic transition between bound states i and j can be defined as $\tau \sim \xi_0 L$, where L is the plasma length and ξ_0 is the line center absorption coefficient

$$\xi_0 \text{ (cm}^{-1}\text{)} \sim n_i \text{ (10}^{14} \text{ cm}^{-3}\text{)} f_{ij} \frac{0.011}{\Delta E \text{ (eV)}}, \quad (1)$$

n_i being the number density of the atomic level i , f_{ij} the oscillator strength of the transition between the bound states i and j and ΔE the full width at half maximum of the line [8]. For typical NSTX divertor conditions, the optical depth τ for B6–B10 lines is ≤ 0.001 . NSTX divertor plasmas are then typically optically thin to Balmer series radiation and radiation transport effects were not included in the CRETIN simulations.

In this limit, CRETIN was employed to solve for collisional–radiative (CR) atomic level populations based on the Johnson–Hinnov atomic model [9]. CRETIN also includes a line shape calculation code, TOTAL, which uses a binary collisional operator for the electrons and a quasi static ion microfield approximation [8]. Line broadening for B6 and B10, obtained convolving the pure Stark profile with thermal (2 eV) and instrumental (0.11 nm) Gaussian profiles, is shown in Fig. 3. Stark broadening of these Balmer lines gives enough sensitivity in the n_e determination for densities above $1 \times 10^{14} \text{ cm}^{-3}$, with increasing sensitivity for higher transitions.

The fitting procedure employed for the analysis of experimentally measured spectra will be now described. After the identification, fitting, and subtraction of impurity lines from the experimental spectrum, a Voigt fitting procedure on the measured data was used to determine the total full width at half maximum (FWHM). The Gaussian component of the Voigt profile was held fixed at the convolution between the instrumental and a 2 eV thermal Gaussian, and the pure Stark component was then fitted. Density values were determined from the Stark FWHM based on CRETIN calculations. In pre-lithium discharges, due to the high divertor n_e and high recombination rate, Stark broadening from transitions B7–B10 was used. In post-lithium discharges, only transitions up to B7 were strong enough to be distinguished from the background; Stark broadening of B6 and B7 was used.

To study the connection between divertor reduced recycling regime and the inner divertor re-attachment, NSTX inner divertor

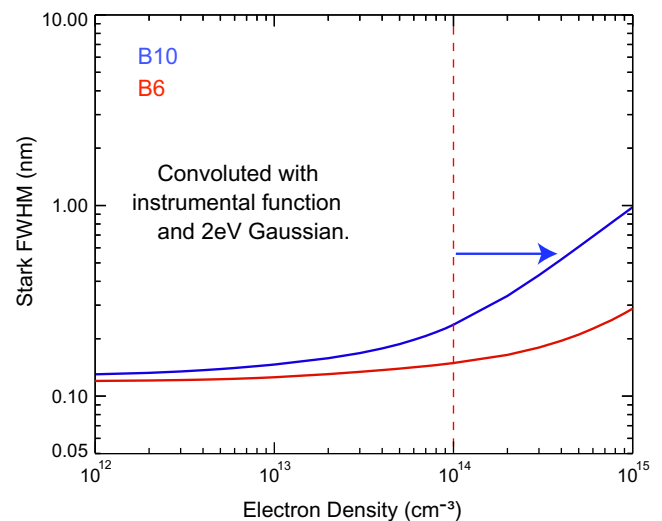


Fig. 3. FWHM as a function of n_e for Balmer 10–2 and 6–2 as calculated by CRETIN. Stark broadening starts dominating the FWHM for densities higher than $1 \times 10^{14} \text{ cm}^{-3}$.

plasmas were simulated using a 1D partially ionized plasma transport model integrated into CRETIN, PIP [4], which includes charge exchange coupling in the transport coefficients and atomic processes rates calculated from the local plasma parameters. PIP was used to simulate a 1D hydrogen plasma 4 m along the magnetic field line from the X-point to the inner divertor target. The simulation included heat flux equally shared between ions and electrons. The upstream electron density was $3 \times 10^{13} \text{ cm}^{-3}$. The transition to re-attachment was chosen at $T_e \geq 1.6 \text{ eV}$ since the ionization rate becomes much greater than the recombination rate. The effect of the pumping provided by lithium coatings was modeled by varying the recycling coefficient at the divertor target.

3. Results and discussion

The effect of lithium coatings on the inner divertor plasmas is evident through the analysis of deuterium high- n Balmer line spectra which show reduced intensity and reduced broadening. In Fig. 4, spectra acquired in a discharge before (black) and after (red) lithium deposition are compared at two different times during the discharge. In pre-lithium discharges Balmer transitions from excited states as high as $n = 11$ can be clearly distinguished, indicating the presence of volumetric recombination. In discharges with lithium coatings, high- n Balmer transitions are absent in the early stage of the discharge but gradually increase in intensity with time (e.g. B9 in Fig. 4a/b, red solid line). Lower transitions (e.g. B6) show greatly reduced Stark broadening. In Fig. 4c, deuterium Balmer spectra simulated by CRETIN, corresponding to the experimental spectra in Fig. 4a, are shown. The best matches were obtained for $T_e = 1 \text{ eV}$ for the pre-lithium case and $T_e \geq 2 \text{ eV}$ for the post-lithium case. It must be noted, also, that molecular background is not included in CRETIN simulations.

n_e measurements based on Stark broadening for the two discharges reported in Fig. 4 are plotted in Fig. 5. In black, n_e inferred from Stark broadening from Balmer transitions are shown for a discharge without lithium coatings. Transitions B7–B10 give results that are consistent with each other and indicate n_e in the mid 10^{14} cm^{-3} range. n_e appears to be more or less constant throughout the discharge. In red, n_e derived from B6 and B7 is shown for a discharge with lithium coatings. Electron density is reduced by as much as 75% from the pre-lithium values in the early stages of the discharge. The large fluctuations in the density measurement are mostly due to plasma MHD events. However, a clear increase in the inner divertor n_e during the discharge can be observed. This suggests progressive passivation of the evaporative lithium coatings; in fact, complete passivation is usually observed in NSTX within 2–3 discharges after the lithium evaporation [10].

A drop in the recombination rate and thus a re-attachment of the inner divertor leg is suggested by the disappearing/weakening of high- n Balmer transitions, the reduced density and the increased target electron temperature ($\sim 1 \text{ eV}$ in pre-lithium discharge, $\geq 2 \text{ eV}$ in post-lithium discharge, Fig. 4c). This conclusion is also supported by the reduced neutral pressure in the divertor area (Fig. 1e).

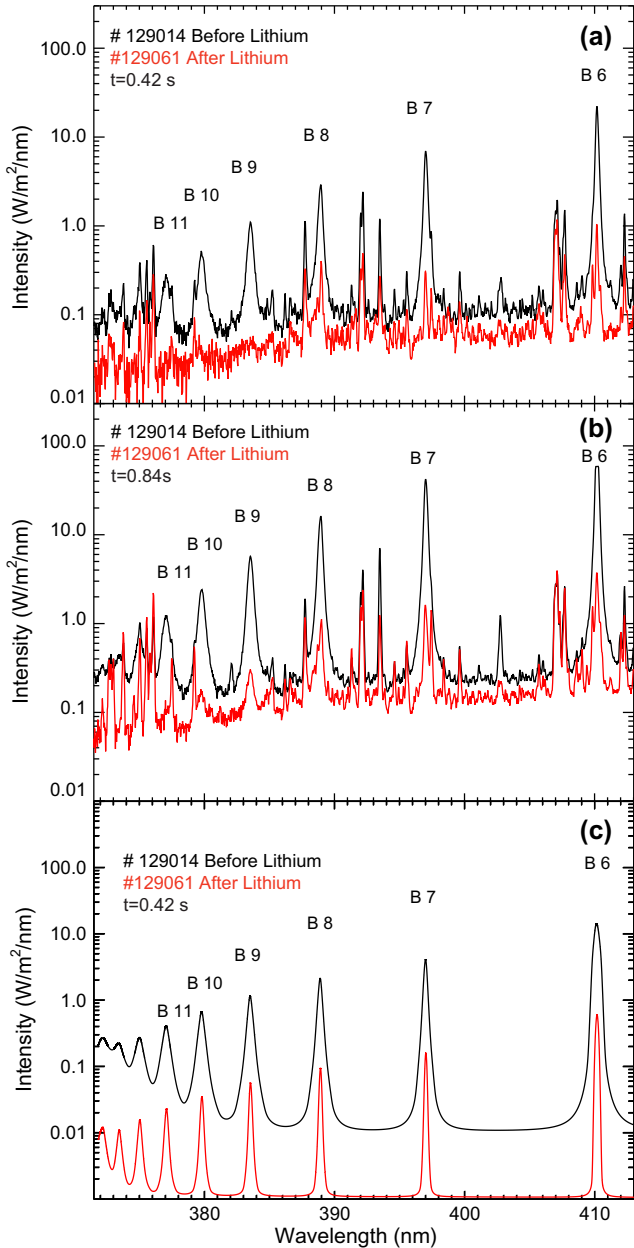


Fig. 4. Spectra acquired through a viewing chord at $R = 0.31 \text{ m}$ at $t = 0.42 \text{ s}$ (a) and at $t = 0.84 \text{ s}$ (b). Spectra from a pre-lithium discharge (#129014) are shown with a black solid line. Spectra from a post-lithium discharge (#129061) are shown with a red solid line. CRETIN simulations are shown in (c). Densities were assumed from Stark broadening measurements ($3.25 \times 10^{14} \text{ cm}^{-3}$ for pre-lithium at $t = 0.42 \text{ s}$, $8.25 \times 10^{13} \text{ cm}^{-3}$ for post-lithium inferred from B6 at a similar time $t = 0.39 \text{ s}$). Electron temperatures were estimated to be $\sim 1 \text{ eV}$ for the pre-lithium case and $\geq 2 \text{ eV}$ for the post-lithium case.

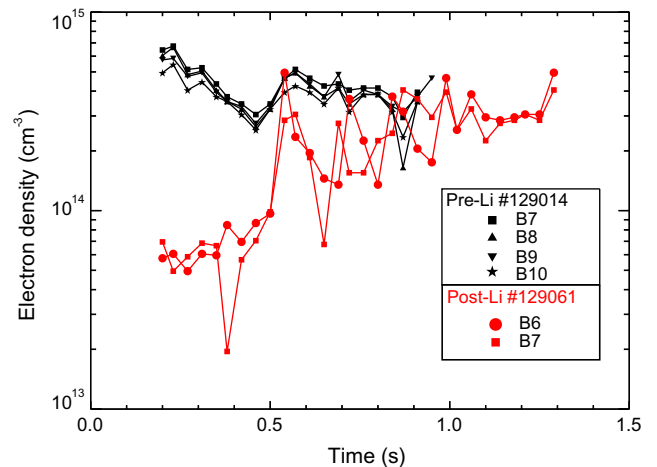


Fig. 5. Inner divertor electron densities evaluated from Stark broadening of different Balmer lines. Densities for a pre-lithium discharge (#129014) are plotted with a black trace. Densities for a post-lithium discharge (#129061) are plotted with a red trace. (For interpretation of the references to color in this figure legend, the reader is referred to the web version of this article.)

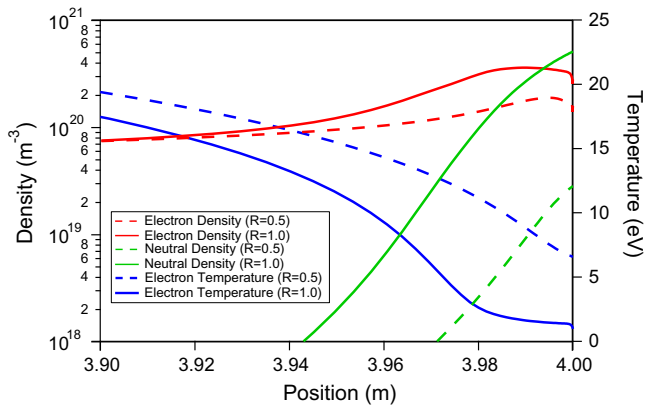


Fig. 6. Electron density, electron temperature and neutral density spatial profiles along the magnetic field line for simulations with recycling coefficient $R = 1.0$ (solid line) and $R = 0.5$ (dashed line) and $q_{\parallel} = 25 \text{ MW/m}^2$. Simulations were carried out for a 1D hydrogen plasma 4 m along the magnetic field line from the X-point ($x = 0 \text{ m}$) to the inner divertor target ($x = 4 \text{ m}$).

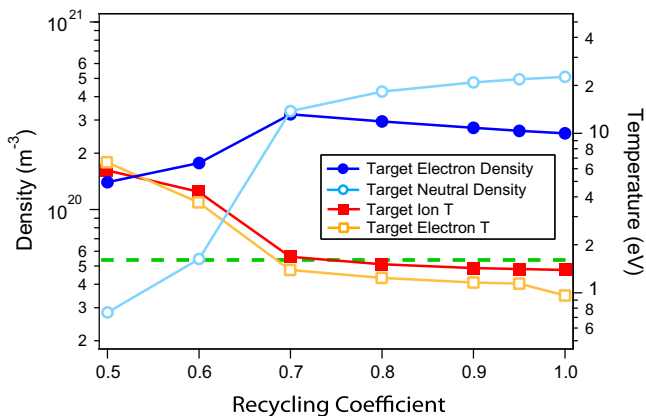


Fig. 7. Target plasma parameters evolution with the change in the recycling coefficient as simulated by PIP for $q_{\parallel} = 25 \text{ MW/m}^2$.

These experimental observations are, qualitatively, confirmed by PIP simulations. Parallel heat flux (q_{\parallel}) scans at different recycling coefficients showed that the change in the recycling affects the downstream divertor regimes (e.g., transition from detached to attached) only for a particular range of parallel heat fluxes (20–30 MW/m^2). For q_{\parallel} lower than these threshold values the divertor plasma was always detached (for values of the recycling coefficient between 0.5 and 1.0 considered in this paper) while for higher values it was always attached. In all simulations, a small increase in the parallel heat flux (above the threshold value) caused a drastic increase in the electron temperature and a decrease in both electron and neutral densities at the target.

The effect of lithium coatings was modeled by reducing the recycling coefficient (from $R = 1.0$ down to $R = 0.5$). For a value of q_{\parallel} of 25 MW/m^2 , a scan of the divertor recycling coefficient was carried out. Profiles of plasma parameters are shown in Fig. 6 for the PIP simulation with $R = 0.5$ and $R = 1.0$. The transition from detached to attached regime appeared to happen for a small change in the recycling coefficient between $R = 0.7$ and $R = 0.6$ for the plas-

ma parameters used in this simulation. The transition value of the recycling coefficient increased with the increase in the parallel heat flux. The effects of the re-attachment were the steeper increase of the electron and ion temperature and the simultaneous decrease in the target electron density and neutral density, as it can be seen in Fig. 7. These results are consistent with what experimentally observed: the absence of high- n Balmer lines and the reduced Stark broadening in post-lithium discharges are consistent with the increase in the electron temperature and decrease in electron density seen in PIP simulations. However, the values obtained for the recycling coefficient at the transition between attached and detached regimes are lower than those obtained in UEDGE simulations for similar discharges [11].

4. Conclusions

The effects of the reduced recycling due to lithium evaporated coatings on the inner divertor regimes of NSTX H-mode discharges have been studied. The inner divertor density was reduced, electron temperature increased and the rate of volumetric recombination processes reduced. This suggested a re-attachment of the inner divertor leg, that was generally detached in pre-lithium discharges. Simulations with a 1D partially ionized plasma code (PIP), qualitatively agreed with experimental results obtained from spectroscopic measurements of deuterium Balmer series transition lines. PIP simulations indicated that the change in the recycling coefficient affects the divertor regimes only within a certain range of parallel heat fluxes. The transition to an attached regime was shown to happen for a small decrease of the recycling coefficient between 0.7 and 0.6.

Acknowledgments

This work was supported by the US DOE under Contracts DE-AC52-07NA27344 and DE-AC02-09CH11466.

References

- [1] ITER Physics Expert Group on Divertor and ITER Physics Expert Group on Divertor Modelling, Nucl. Fusion 39 (1999) 1391.
- [2] V.A. Soukhanovskii, R. Maingi, A.L. Roquemore, J. Boedo, C. Bush, R. Kaita, H.W. Kugel, B.P. LeBlanc, S.F. Paul, G.D. Porter, N.S. Wolf, J. Nucl. Mater. 337–339 (2005) 475–479.
- [3] H.W. Kugel, M.G. Bell, J.P. Allain, R.E. Bell, S.P. Gerhardt, M.A. Jaworski, R. Kaita, J. Kallman, S.M. Kaye, B.P. LeBlanc, R. Maingi, R. Majeski, R. Maqueda, D.K. Mansfield, R. Nygren, R. Raman, A.L. Roquemore, H. Schneider, C.H. Skinner, V.A. Soukhanovskii, C.N. Taylor, J.R. Timberlake, L.E. Zakharov, S.J. Zweben and the NSTX Research Team, These proceedings.
- [4] M.L. Adams, H.A. Scott, Contrib. Plasma Phys. 44 (2004) 262.
- [5] H.A. Scott, J. Quant. Spectrosc. Rad. Transfer 71 (2–6) (2001) 689–701.
- [6] V.A. Soukhanovskii, D.W. Johnson, R. Kaita, A.L. Roquemore, Rev. Sci. Instrum. 77 (2006) 10127.
- [7] R. Raman, H.W. Kugel, R. Gernhardt, T. Provost, T.R. Jarboe, V. Soukhanovskii, Rev. Sci. Instrum. 75 (10) (2004) 4347–4349.
- [8] M.L. Adams, R.W. Lee, H.A. Scott, H.K. Chung, L. Klein, Phys. Rev. E 66 (2002) 066413.
- [9] L.C. Johnson, E. Hinnov, J. Quant. Spectrosc. Rad. Transfer 13 (4) (1973) 333–358.
- [10] H.W. Kugel, M.G. Bell, J.-W. Ahn, J.P. Allain, R. Bell, J. Boedo, C. Bush, D. Gates, T. Gray, S. Kaye, R. Kaita, B. LeBlanc, R. Maingi, R. Majeski, D. Mansfield, J. Menard, D. Mueller, M. Ono, S. Paul, R. Raman, A.L. Roquemore, P.W. Ross, S. Sabbagh, H. Schneider, C.H. Skinner, V. Soukhanovskii, T. Stevenson, J. Timberlake, W.R. Wampler, L. Zakharov, Phys. Plasmas 15 (2008) 056118.
- [11] R.D. Smirnov, A.Yu. Pigarov, S.I. Krashennnikov, T.D. Rognien, V.A. Soukhanovskii, M.E. Rensink, R. Maingi, C.H. Skinner, D.P. Stotler, R.E. Bell, H.W. Kugel, Contrib. Plasma Physics 50 (2010) 299.